

Article

Analysis of Heat Transfer Behavior of Porous Wavy Fin with Radiation and Convection by Using a Machine Learning Technique

Chandan Kumar ^{1,†} , P. Nimmy ¹, Kallur Venkat Nagaraja ¹ , R. S. Varun Kumar ¹, Amit Verma ², Shalan Alkarni ³ and Nehad Ali Shah ^{4,*,†}

- ¹ Department of Mathematics, Amrita School of Engineering, Amrita Vishwa Vidyapeetham, Bengaluru 560035, India; chandanrko786@gmail.com (C.K.); bl.sc.r4mat22010@bl.students.amrita.edu (P.N.); kv_nagaraja@blr.amrita.edu (K.V.N.); rs_varun@blr.amrita.edu (R.S.V.K.)
- ² University Centre for Research & Development, Department of Computer Science & Engineering, Chandigarh University, Gharuan, Mohali 140413, India; amit.e9679@cumail.in
- ³ Department of Mathematics, College of Sciences, King Saud University, P.O. Box 2455, Riyadh 11451, Saudi Arabia; shalkarni@ksu.edu.sa
- ⁴ Department of Mechanical Engineering, Sejong University, Seoul 05006, Republic of Korea
- * Correspondence: nehadali199@sejong.ac.kr
- † These authors contributed equally to this work and are co-first authors.

Abstract: The impact of convection and radiation on the thermal distribution of the wavy porous fin is examined in the present study. A hybrid model that combines the differential evolution (DE) algorithm with an artificial neural network (ANN) is proposed for predicting the heat transfer of the wavy porous fin. The equation representing the thermal variation in the wavy porous fin is reduced to its dimensionless arrangement and is numerically solved using Rung, e-Kutta-Fehlberg's fourth-fifth order method (RKF-45). The study demonstrates the effectiveness of this hybrid model, and the results indicate that the proposed approach outperforms the ANN model with parameters obtained through grid search (GS), showcasing the superiority of the hybrid DE-ANN model in terms of accuracy and performance. This research highlights the potential of utilizing DE with ANN for improved predictive modeling in the heat transfer sector. The originality of this study is that it addresses the heat transfer problem by optimizing the selection of parameters for the ANN model using the DE algorithm.

Keywords: heat transfer; fin; porous fin; wavy fin; machine learning; differential evolution



Citation: Kumar, C.; Nimmy, P.; Nagaraja, K.V.; Kumar, R.S.V.; Verma, A.; Alkarni, S.; Shah, N.A. Analysis of Heat Transfer Behavior of Porous Wavy Fin with Radiation and Convection by Using a Machine Learning Technique. *Symmetry* **2023**, *15*, 1601. <https://doi.org/10.3390/sym15081601>

Academic Editors: Yifei Guan and Jian Wu

Received: 27 July 2023

Revised: 14 August 2023

Accepted: 15 August 2023

Published: 18 August 2023



Copyright: © 2023 by the authors. Licensee MDPI, Basel, Switzerland. This article is an open access article distributed under the terms and conditions of the Creative Commons Attribution (CC BY) license (<https://creativecommons.org/licenses/by/4.0/>).

1. Introduction

Heat transfer has become a significant subject in the field of thermal engineering. There has been an increase in demand for improved thermal systems that provide a better heat transfer rate in industrial applications. Due to spatial temperature differences, the transmission of thermal energy, termed heat transfer, occurs within or between mediums in three modes: heat conduction, radiation, and convection. Many researchers have inspected the aspects of heat transmission and its applications. Jo et al. [1] studied the heat transfer mechanism of a pulsating heat pipe. Their results revealed that sensible heat transfer is a byproduct of oscillating flow, whereas latent heat transfer contributes to the overall heat transfer and encourages an oscillating flow. The convective heat transfer characteristics of a porous medium in a heat exchanger were investigated by Hu et al. [2]. Their results conveyed that overall heat transfer performance decreases as velocity increases, and the heat transfer coefficient, pressure drop, and the volumetric heat transfer coefficient increase along with an increase in the number of cells per inch. The convection–radiation heat transfer process of a chip embedded in an enclosure was studied by Hassan and Shafey [3]. The study concluded that as the input power induced by the chip increases,

the chip's temperature would also increase. Combined mixed convective and surface radiation heat transmission inside an air-filled enclosure was investigated by Prakash and Singh [4]. Their results indicate that the heat removal rate is augmented as the velocity near the active wall increases. Zhang and Lou [5] validated an improvised thermodynamic analysis method to evaluate the efficiency and irreversibility of the radiative–conductive heat transfer process. Their findings indicate that, as the heat generation rate increases, total exergy increases, and the amount of heat generation exhibits more prominence on the radiative entropy generation rate. Without affecting the overall performance of the heat transfer devices, different techniques have been implemented in the ever-demanding industrial sector to augment the heat transfer processes, such as the following: insertion of twisted tapes, wire coils, coating of surfaces, applications of nanofluids, provision of rough or porous surfaces, coupling of an electrical or magnetic field, impingement of jets, and suction. The heat transfer rate can be characteristically increased with an increased heat transfer coefficient, heat exchanging area, and temperature difference. However, owing to technical limitations, it is inadvisable to escalate the temperature difference significantly, and increasing the heat transfer coefficient is a major risk. Thus, expanding the heat transference area seems to be one of the finest ways to augment the heat exchange rate. Accordingly, a thin metal strip, called a fin, or an extended surface, is attached to the base surface of the heat-transferring devices. Fins are broadly exploited in electronic components, car radiators, pipelines, turbine blades, electrical chips, compressors, refrigerators, solar collectors, and heat sinks. Differential equations are generally utilized to represent various natural phenomena in many disciplines, including physics, biology, and engineering. The heat transfer equations of the fins are also represented by nonlinear differential equations (NDEs). The most significant of the several applications of modern mathematical theories is the complex and important study of NDE systems with symmetries. Interpreting the features of differential equations can be facilitated by using symmetry analysis, particularly when dealing with equations derived from mathematical concepts. Symmetry analysis is a powerful tool that enables effective production of numerical solutions to a given NDE. Examining a naturally occurring phenomenon with the assistance of symmetry analysis is more convenient. Several studies have analyzed the heat transfer performance through various fin profiles by providing a governing NDE. The transient heat transfer process through fins having different profiles was studied by Ndlovu [6] by implementing the differential transform method. The results illustrated that, compared to a fin having an insulated tip, one with a convective radiative tip dissipates more heat rapidly to the surroundings. El Ghandouri et al. [7] presented a new fin shape to improve the convective heat transfer and reduce the weight of heat sinks. Their results indicated that rippling fins resulted in better enhancement of heat transfer, compared to rectangular fins. Li et al. [8] proposed several types of three-dimensional perforated fins to investigate the impact of perforated fins in a latent thermal energy storage system. Their results revealed that a perforated fin better encourages the heat transfer mechanism of phase-changing materials. By applying perforated fins, it was found that the flow area expands, which helps to improve natural convection processes. The heat transfer enhancement within a turbine blade using a curved pin fin was elucidated by Luo et al. [9]. According to the findings of their investigations, it was discovered that, compared to upright pin fins, curved pin fins showed better thermal performance. Under natural convection, Dogmaz et al. [10] investigated the thermal performance of aluminum and functionally graded annular fins. They concluded that the net heat transfer rate increases as the fin spacing decreases. Compared to aluminum fins, functionally graded fins have a superior heat transfer rate, better fin effectiveness and better base to ambient temperature difference.

In recent years, numerous researchers have been interested in the transmission of heat through a medium in which a solid matrix is interlinked with pores. This matrix with pore interlinkages is a porous medium that helps in heat transmission. By permitting the fluid to propagate across the whole domain, and by transmitting heat from one part to another, the pore spaces created by the medium's matrix organization contribute to

convective heat transfer and a fluid convective mode. As a result, porous fins, falling under the category of passive heat transfer enhancement procedures, have been widely used to boost thermal performance because they perform better and have a larger surface area than conventional solid fins. Due to their ease of applicability in various forms, many researchers have studied the heat dissipation mechanism through porous fins. The concept of employing a porous fin to augment heat transfer from a given porous medium was first introduced by Kiwan and Al-Nimr [11]. They compared and estimated the thermal performance of porous fins and solid fins, and the results showed that using porous fins with a certain porosity could increase the performance of a solid fin of the same size. Using the variational iteration method, the variation of fin efficiency and temperature distribution of a rectangular porous fin was investigated by Ndlovu and Moitsheki [12]. Their results revealed that, by increasing the porous parameter, the temperature decreased, due to the changes in permeability; high porosity resulted in a higher heat transfer rate. By considering internal heat generation, the transient heat transfer along a radiative–convective porous fin was investigated by Emamifar et al. [13]. According to their findings, lowering the convective heat coefficient, or increasing Rayleigh or Darcy number, results in an increase in porosity, which causes a decline in the thermal distribution within the porous fin, and, thus, the heat transfer from the fin is boosted. Das and Kundu [14] demonstrated an inverse methodology by employing the Artificial Bee Colony algorithm to predict internal heat generation in a radial porous fin. They found that internal heat generation greatly impacts the heat transfer rate for lower porosity values. In a differentially heated chamber, Xuan Hoang Khoa et al. [15] investigated the impacts on heat transfer performance of both porous and solid fins. They concluded that, compared to solid fins, the porous fin is more effective in heat elimination. Thermal analysis of a porous fin with outward fluid flow was conducted by Abbas et al. [16]. They noticed that the optimal porosity, which improves the heat removal rate, depends on the period in which the fin removes the heat.

Incorporating geometrically modified fins, comprising louvred fins, offset strip fins, and wavy or corrugated fins, increases the surface area density, while improving the convection heat transfer coefficient. Owing to convenience in usage and production, and the potential for higher thermal–hydraulic performance among these modified fins, wavy fins symmetric around the length or width axis, are the most attractive. The corrugated shape of these symmetric fins facilitates the expansion of the surface area in the available space, amplifying the flow distortion and mixing. Numerous investigations have been conducted on the thermal performance of wavy fins. Convective–radiative heat transfer in a wavy sinusoidal fin was investigated by Altun and Ziylan [17]. Their results indicated that, compared to rectangular fins, sinusoidal wavy fins showed better heat transfer performance. Luo et al. [18] studied different corrugation angles on wavy fins. Their findings indicated that incorporating a novel wavy fin improved heat transfer performance. The thermal performance of a wavy fin comprised of rectangular winglets in air conditioners was studied by Chimres et al. [19]. They compared the thermal performance of the wavy fin having winglets with a normal wavy fin. Their results revealed that wavy fins having winglets provided a better heat transfer rate than normal wavy fins. A new design for a heat sink having porous wavy fins, named wavy-top-porous fins (WTPF), was proposed by Boland and Majidi [20]. They compared this proposed WTPF with other fin configurations and concluded that WTPF showed the best overall thermal performance among the configurations. Okon and Effiom [21] determined the thermal performance of wavy fin arrays. Their results disclosed that the amount of heat transferred depends upon the fin’s space, height, wavelength and base to ambient temperature. They also found that, in comparison to rectangular fin arrays, wavy fin arrays possessed greater convection heat transfer performance.

To predict and analyze heat transfer phenomena in augmenting the design structure of heat transfer systems and optimizing heat transmission processes, artificial intelligence-based machine learning (ML) techniques are widely utilized nowadays. Apart from this, ML models are implemented to investigate the abundant data generated from experiments,

simulations and field observations. As a whole, ML techniques boost the accuracy and effectiveness of data, and further examination of these methods will result in major advancements in the heat transfer domain. By the application of a radial basic function (RBF) network, Alizadeh et al. [22] investigated the heat and mass transfer over a porous medium. Their study illustrated that variation in radiative heat transfer impacts the heat and mass transfer responses. It also demonstrated how ML can facilitate resolving matters involving abundant parameters by lowering the required computations. The K-Nearest Neighbor, an ML algorithm, was employed by Krishnayatra et al. [23] to predict a fin's thermal performance. The result concluded that this regression model resulted in greater prediction accuracy. With the aid of a Genetic algorithm and pix2pix networks, Yang et al. [24] optimized the arrangement and shape of a pin fin array. They trained and tested the model in predicting the thermal and pressure distributions on the channel. Their results revealed that, to regress the exterior surface temperature and the pressure distribution in the middle section, the pix2pix model was the appropriate network type among the pin fin channels. To study the temperature distribution through porous fins having different fin profiles, the ML algorithm, namely the Levenberg–Marquardt (LM) algorithm, and cascade feedforward back propagated (CFB) neural networks, was employed by Khan et al. [25]. They compared the above-mentioned algorithm with other ML algorithms, and the resulting solution reflected a minimum error between 10^{-6} and 10^{-10} . Optimization in the shape of a pin fin using a genetic algorithm coupled with the ML model was reported by Nguyen et al. [26]. During the design process, they used an ML model to evaluate the pressure and temperature caused by the fins within a second. The results verified that ML-based optimization techniques can be utilized to find undiscovered heat transfer system shapes that perform better.

Heat transfer is essential in many manufacturing and scientific operations, notably heat exchangers, combustors, computer processors, fuel cells, and gas turbine blades. On the other hand, artificial intelligence-based ML methodologies are employed to determine engineering challenges in almost every industry concerning heat transfer mechanisms. Differential evolution (DE), prevalent in various scientific and technical domains, has emerged as a highly effective population-based stochastic search strategy for addressing optimization issues across a continuous space. Stimulated by these facts, a machine learning technique based on differential evolution was employed to establish a fin's heat transfer model. Furthermore, the current study is innovative in addressing the thermal behavior and heat transmission of a porous wavy fin under the coupled influence of radiation and convection. The proposed nonlinear problem was transformed into a non-dimensional ODE by adopting dimensionless variables. This study examined the significance of several parameters on the temperature field and the heat transfer rate graphically. The findings offer better comprehension of heat transmission in porous structures with wavy fins, which can be helpful in various technical and industrial applications, such as, for instance, heat exchanger design.

2. Formulation of the Problem

The steady-state heat transmission in a porous wavy fin (PWF) of width W and height $2H$, symmetric around the length axis, is investigated. The considered PWF is geometrically represented and is revealed in Figure 1. The primary presumptions for the current problem are outlined below:

- The proposed fin geometry is symmetric around the length axis and wavy along the x-direction.
- It is presumed that the temperature varies only longitudinally and does not vary across the thickness.
- Convection and radiation heat transfer with constant ambient temperature T_{AMB} are considered to be the heat-exchanging mechanism of PWF.
- The porous medium, which is homogeneous and isotropic, is saturated with a single-phase fluid.

- The fin tip is assumed to be adiabatic, comparable to ignoring the fin tip transferring heat due to its minimal area.

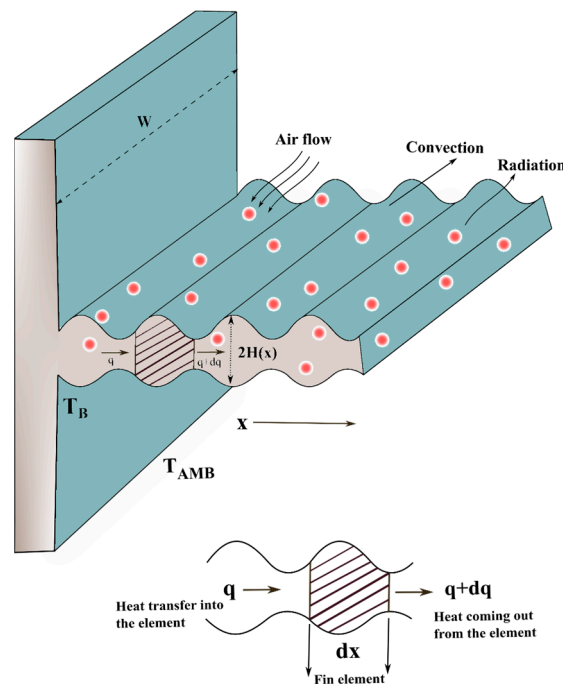


Figure 1. Graphical illustration of a porous wavy fin.

The dimensional energy equation for the PWF is obtained as follows (Sowmya et al. [27] and Kumar et al. [28]):

$$\begin{aligned} \frac{d}{dx} \left[k_{eff} \frac{dT_{WF}}{dx} \right] &= (1 - \phi) \left[\frac{dA_{SF}}{dx} \right] \frac{h^*(T_{WF})}{A_{CS}} (T_{WF} - T_{AMB}) - \left[\frac{k_{eff}}{A_{CS}} \frac{dA_{CS}}{dx} \right] \frac{dT_{WF}}{dx} \\ &+ \left[\frac{dA_{SF}}{dx} \right] \frac{\sigma \epsilon^*}{A_{CS}} (T_{WF}^4 - T_{AMB}^4) + \left[\frac{dA_{SF}}{dx} \right] \frac{\phi}{A_{CS}} \frac{\rho_f c_{pf} g K \beta_f}{\nu_f} (T_{WF} - T_{AMB})^2. \end{aligned} \quad (1)$$

Here, both solid and fluid thermal conductivities (k_{sd} and k_f) collectively influence the effective thermal conductivity (k_{eff}) which is denoted as:

$$k_{eff} = k_f \phi + k_{sd}(1 - \phi), \quad (2)$$

and $h^*(T_{WF})$ depends on the temperature of the PWF, as well as the ambient temperature, which is mathematically represented as (Abdulrahman et al. [29]):

$$h^*(T_{WF}) = h_b \left(\frac{T_{WF} - T_{AMB}}{T_B - T_{AMB}} \right)^\xi. \quad (3)$$

Substituting Equations (2) and (3) in Equation (1) yields,

$$\begin{aligned} \frac{d}{dx} \left[(k_f \phi + k_{sd}(1 - \phi)) \frac{dT_{WF}}{dx} \right] &+ (k_f \phi + k_{sd}(1 - \phi)) \frac{dT_{WF}}{dx} \left[\frac{1}{A_{CS}} \frac{dA_{CS}}{dx} \right] - \\ (1 - \phi) \frac{1}{A_{CS}} \left[\frac{dA_{SF}}{dx} \right] \frac{h_b (T_{WF} - T_{AMB})^{\xi+1}}{(T_B - T_{AMB})^\xi} &- \left[\frac{dA_{SF}}{dx} \right] \frac{\sigma \epsilon^*}{A_{CS}} (T_{WF}^4 - T_{AMB}^4) \\ - \left[\frac{dA_{SF}}{dx} \right] \frac{\phi}{A_{CS}} \frac{\rho_f c_{pf} g K \beta_f}{\nu_f} (T_{WF} - T_{AMB})^2 &= 0. \end{aligned} \quad (4)$$

The fin half height H and cross-sectional area of the PWF are given by

$$H = H_0 \left\{ 1 + \delta \sin \left[2\pi n \left(\frac{x}{L} \right) + \phi \right] \right\}, \quad (5)$$

and

$$A_{CS} = 2H_0 \int_0^W \left\{ 1 + \delta \sin \left[2\pi n \left(\frac{x}{L} \right) + \varphi \right] \right\} dz, \quad (6)$$

where, W denotes the width of the PWF.

The PWF surface area is provided by

$$A_{SF} = 2W \int_0^L \sqrt{1 + \left(\frac{dH}{dx} \right)^2} dx. \quad (7)$$

Here, $L_{ta} = \int_0^L \sqrt{1 + \left(\frac{dH}{dx} \right)^2} dx$ is the total arc length of the PWF.

Equation (4) is associated with the following boundary conditions:

$$\begin{aligned} x = 0 : T_{WF} &= T_B, \\ x = L : \frac{dT_{WF}}{dx} &= 0. \end{aligned} \quad (8)$$

By defining the subsequent dimensionless terms,

$$\begin{aligned} \Theta_{WF} &= \frac{T_{WF} - T_{AMB}}{T_B - T_{AMB}}, \quad X = \frac{x}{L}, \quad N_t = \frac{T_{AMB}}{T_B - T_{AMB}}, \quad Nc = \frac{h_b L^2}{k_{sd} H_0}, \quad a_{RL} = \frac{H_0}{L}, \quad k_r = \frac{k_f}{k_{sd}}, \\ Nr &= \frac{\sigma \varepsilon^* L^2 (T_B - T_{AMB})^3}{k_{sd} H_0}, \quad Sh = \frac{\rho_f c_{pf} g K \beta_f L^2 (T_B - T_{AMB})}{k_{sd} \nu_f H_0}, \end{aligned} \quad (9)$$

the corresponding dimensionless energy equation is obtained:

$$\begin{aligned} &((1 - \phi) + \phi k_r) \frac{d^2 \Theta_{WF}}{dX^2} + ((1 - \phi) + \phi k_r) \left[\frac{2\pi \delta n \cos(2\pi n X + \varphi)}{1 + \delta \sin(2\pi n X + \varphi)} \right] \frac{d\Theta_{WF}}{dX} - \\ &(1 - \phi) Nc \left[\frac{\sqrt{1 + 4(\pi a_{RL} \delta n)^2 \cos^2(2\pi n X + \varphi)}}{1 + \delta \sin(2\pi n X)} \right] \Theta_{WF}^{\zeta+1} \\ &- \phi Sh \left[\frac{\sqrt{1 + 4(\pi a_{RL} \delta n)^2 \cos^2(2\pi n X + \varphi)}}{1 + \delta \sin(2\pi n X)} \right] \Theta_{WF}^2 \\ &- Nr \left[\frac{\sqrt{1 + 4(\pi a_{RL} \delta n)^2 \cos^2(2\pi n X + \varphi)}}{1 + \delta \sin(2\pi n X)} \right] \left((\Theta_{WF} + N_t)^4 - N_t^4 \right) = 0. \end{aligned} \quad (10)$$

The BC for Equation (10) is specified as:

$$\begin{aligned} X = 0 : \Theta_{WF} &= 1, \\ X = 1 : \frac{d\Theta_{WF}}{dX} &= 0. \end{aligned} \quad (11)$$

The dimensionless thermal equation is solved using RKF-45 and the substitutions mentioned below are used to convert Equation (10) into a first-order ODE.

$$\begin{cases} \Theta_{WF} = E, \\ \frac{d\Theta_{WF}}{dX} = E_1, \\ \frac{d^2 \Theta_{WF}}{dX^2} = E_2 \end{cases} \quad (12)$$

Then, the equivalent form of Equation (10), with the above-specified terms, is given by,

$$E_2 = \frac{1}{((1 - \phi) + \phi k_r)} \left[\begin{array}{l} -((1 - \phi) + \phi k_r) \left[\frac{2\pi\delta n \cos(2\pi n X + \phi)}{1 + \delta \sin(2\pi n X + \phi)} \right] E_1 + \\ Nc \left[\frac{\sqrt{1 + 4(\pi a_{RL} \delta n)^2 \cos^2(2\pi n X + \phi)}}{1 + \delta \sin(2\pi n X)} \right] E^{\xi+1} + \\ Nr \left[\frac{\sqrt{1 + 4(\pi a_{RL} \delta n)^2 \cos^2(2\pi n X + \phi)}}{1 + \delta \sin(2\pi n X)} \right] \left((E + N_t)^4 - N_t^4 \right) \\ + Sh \left[\frac{\sqrt{1 + 4(\pi a_{RL} \delta n)^2 \cos^2(2\pi n X + \phi)}}{1 + \delta \sin(2\pi n X)} \right] E^2 \end{array} \right], \tag{13}$$

with BCs:

$$E(0) = 1, E_1(1) = 0. \tag{14}$$

The following steps are taken to obtain the numerical solution:

$$\begin{aligned} \gamma_1 &= hG(\eta_\gamma, \omega_\gamma), \\ \gamma_2 &= hG(\eta_\gamma + \frac{1}{4}h, \omega_\gamma + \frac{1}{4}\gamma_1), \\ \gamma_3 &= hG(\eta_\gamma + \frac{3}{8}h, \omega_\gamma + \frac{3}{32}\gamma_1 + \frac{9}{32}\gamma_2), \\ \gamma_4 &= hG(\eta_\gamma + \frac{12}{13}h, \omega_\gamma + \frac{1932}{2197}\gamma_1 - \frac{7200}{2197}\gamma_2 + \frac{7296}{2197}\gamma_3), \\ \gamma_5 &= hG(\eta_\gamma + h, \omega_\gamma + \frac{439}{216}\gamma_1 - 8\gamma_2 + \frac{3680}{513}\gamma_3 - \frac{845}{4104}\gamma_4), \\ \gamma_6 &= hG(\eta_\gamma + \frac{1}{2}h, \omega_\gamma - \frac{8}{27}\gamma_1 + 2\gamma_2 - \frac{3544}{2565}\gamma_3 + \frac{1859}{4104}\gamma_4 - \frac{11}{40}\gamma_5). \end{aligned} \tag{15}$$

The RK-4 approach was used to approximate a solution to the aforementioned initial value problem.

$$\omega_{\gamma+1} = \omega_\gamma + \frac{25}{216}\gamma_1 + \frac{1408}{2565}\gamma_3 + \frac{2197}{4101}\gamma_4 - \frac{1}{5}\gamma_5,$$

and the RK-5 method is being used to improve the value of the solution:

$$Z_{\gamma+1} = \omega_\gamma + \frac{16}{135}\gamma_1 + \frac{6656}{12825}\gamma_3 + \frac{28561}{56430}\gamma_4 - \frac{9}{50}\gamma_5 + \frac{2}{55}\gamma_6. \tag{16}$$

A shooting strategy can be used with suitable parameter quantities to solve the transformed first-order ODE (Equation (13)).

The heat transmission through the PWF is determined by utilizing Fourier’s law at the fin’s base, and is defined as follows:

$$q_{WF} = -k_{eff} \left[\int_0^W H(x = 0, z) dz \right] \frac{dT_{WF}}{dx} \Big|_{x=0}. \tag{17}$$

Equation (17) can be represented using Equation (2) as,

$$q_{WF} = -\left(k_f \phi + k_{Sd}(1 - \phi) \right) WH_0 \frac{dT_{WF}}{dx} \Big|_{x=0}. \tag{18}$$

The non-dimensional form of Equation (18) is given as:

$$\begin{aligned} Q_{WF} &= \frac{q_{WF}}{k_{Sd}(T_B - T_{AMB})W}, \\ &= -((1 - \phi) + \phi k_r) a_{RL} \frac{d\Theta_{WF}}{dX} \Big|_{X=0}. \end{aligned} \tag{19}$$

3. Stochastic Machine Learning Modeling

3.1. Artificial Neural Networks

Artificial neural networks (ANNs) are popular ML approaches that extract relevant features from high-dimensional input data samples. Stimulated by the working of the human brain, ANNs simulate the process of learning and pattern recognition, which is advantageous for solving several complex problems. In comparison to traditional statistical regression methods, ANN exhibits superior predictive ability and can autonomously identify meaningful patterns and features in data without prior knowledge or explicit insight (Cui et al. [30] and Goud et al. [31]). Additionally, they can iteratively improve performance over many training cycles and rapidly estimate overall statistics when applied to datasets containing numerous variables. In the domain of heat transfer research, the concept of ANN has risen to prominence as a remarkable tool for the management of complexities of intricate systems (Motahar [32] and Kumar et al. [33]). The modeling of ANN structures is similar to virtual brains and is meticulously developed with input, hidden, and output layers, resulting in a highly interconnected network. A rigorous testing process ensures the network's efficacy, where independent test data are carefully kept separate from the training phase. This meticulous evaluation safeguards against the overfitting condition, and the precise selection of network parameters is an important factor that unravels the ANN model's remarkable ability to perform efficiently.

3.2. Grid Search

Grid Search (GS) is a systematic approach to parameter estimation that involves defining a grid of values for each hyperparameter and exhaustively evaluating the model's performance on each combination of parameter values. It also provides a comprehensive exploration of the parameter space. It ensures that every combination is noticed, and this is particularly useful when prior knowledge or intuition suggests specific values for the hyperparameters. The tuning hyperparameters must each be specified with discrete values (Tikadar and Kumar [34]). The flexibility of GS to examine a wide variety of parameter values without any prior assumptions or limits is its primary advantage. On the other hand, it may suffer from inherent unpredictability because certain values guide the search process, so many iterations may be necessary to converge to an ideal parameter configuration.

3.3. Differential Evolution

There have been efforts to resolve a few of ANN's drawbacks, such as unwanted convergence to local rather than global optimal solutions and a lengthy training period. This can be done by incorporating ANN with another algorithm that addresses a particular issue. Differential Evolution (DE) is a well-known evolutionary technique that was developed by Storn to solve the Chebyshev polynomial fitting issue (Storn [35]). Like other evolutionary algorithms, it has gained substantial attention as a powerful optimization algorithm. In contrast to gradient-based optimization approaches, DE does not need an estimation of gradients; thereby rendering it ideal for non-differentiable or noisy objective functions. When compared to other evolution methods, such as the genetic algorithm and particle swarm optimization, DE's mutation and crossover operators frequently create a good balance between exploration and exploitation, which can help in handling parameter sensitivities effectively. This is especially important in ANN training, where changing parameters can have a big impact on model performance. DE also uses a population-based approach, including separate mutation, crossover, and selection processes. On the other hand, DE distinguishes itself with its amazing ease of implementation, requiring fewer parameters and demonstrating rapid convergence (Centeno-Telleria et al. [36]). Inspired by natural selection principles, DE adeptly solves global optimization challenges, such as parameter estimation, within ANN models (Atangana Njock et al. [37]). By maintaining a population of candidate solutions, DE iteratively refines and evolves these individuals by assimilating the information from the most adept individuals in the population.

The DE process is executed in multiple discrete steps, as exhibited in Figure 2. To begin, critical parameters, such as population size (N), mutation factor (F), and crossover rate (R), must be specified during the initiation phase. Furthermore, in the context of ANN, a chromosome is constructed using three distinct parameters: C_1 , m_1 , and r_1 . These factors specify the length of a chromosome, which, in this case, was three. N was set to 100, whereas F and R were set to 0.5 and 0.9, respectively.

$$M_{\zeta_1 \zeta_2} = rand.(upper[\zeta_2] - lower[\zeta_2]) + lower[\zeta_2]. \tag{20}$$

$$M_i' = M_i + F(M_j - M_i). \tag{21}$$

$$\begin{cases} M_j'(\zeta_2) = M_i'(\zeta_2) & \text{if } rand(\zeta_2) \leq C_1 \text{ or } \zeta_2 = rand(\zeta_2) \\ M_j'(\zeta_2) = M_i(\zeta_2) & \text{otherwise} \end{cases} \tag{22}$$

$$X_{\zeta_2, G+1} = \begin{cases} U_{\zeta_2, G} : f(U_{i, G}) < f(M_{\zeta_2, G}) \\ M_{\zeta_2, G} : \text{otherwise} \end{cases} \tag{23}$$

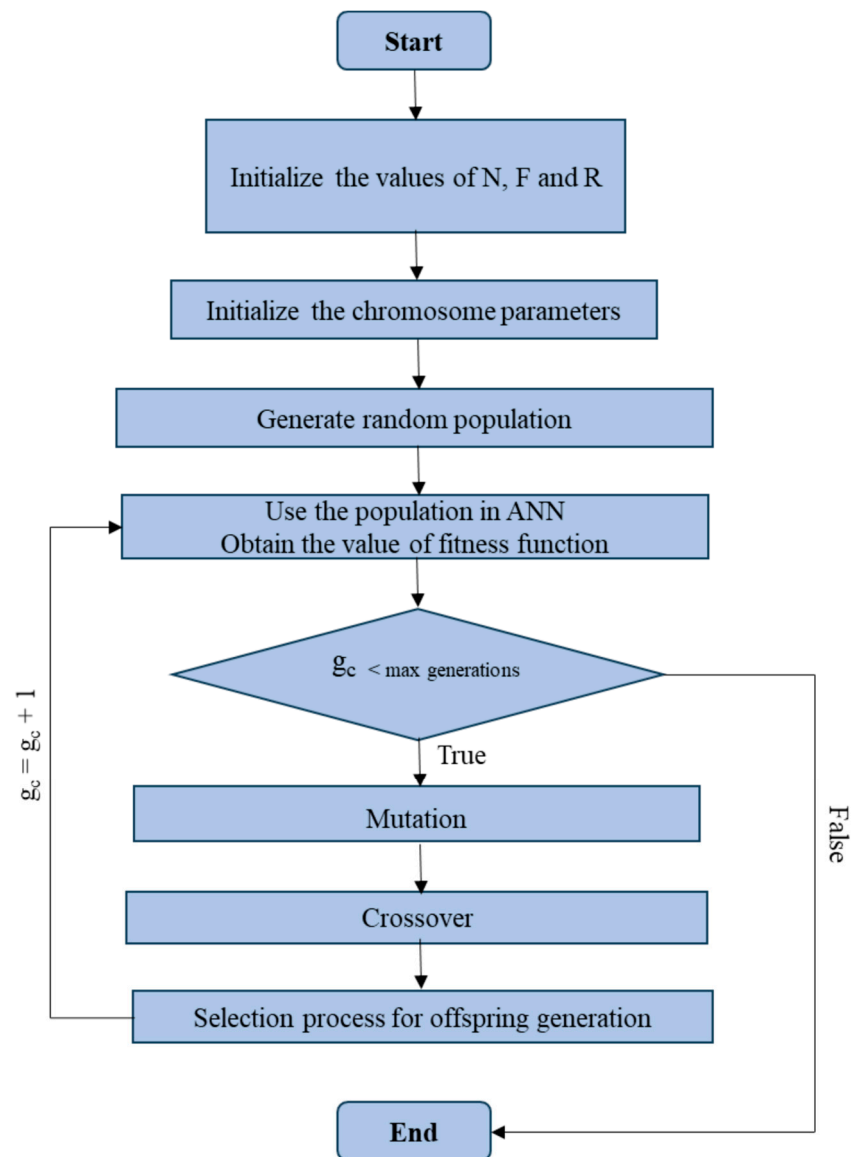


Figure 2. Workflow of the DE-ANN model.

The evolutionary process begins once the parameters are determined. The generation count (g_c) is initially set to zero. The population is then randomly produced using Equation (20), resulting in the initial set of samples. The produced population is then used in the ANN model to forecast optimal results. The fitness function values are calculated and recorded to determine the accuracy of the results. This investigation used the mean squared error (MSE) as the fitness function. After the preliminary computations, offspring are generated using Equations (21)–(23), which include mutation, crossover, and selection activities. These offspring then determine the predictions in the ANN model, allowing updated fitness values to be calculated. Setting up $g_c = g_c + 1$ increases the generation count, indicating the end of one iteration. The iteration procedure is repeated, recalculating fitness values, based on the offspring, and identifying the best solution. This process is repeated until a termination requirement is reached. The method terminates if the g_c equals the predefined maximum number of generations. The best solution chromosome is acquired at this point, indicating the optimal parameter values for the ANN model. If the termination requirement is not encountered, the algorithm returns to the step of recalculating fitness values and the iterative process is resumed. The DE algorithm effectively optimizes the parameters of the ANN model by rigorously following these phases, resulting in accurate predictions.

4. Results and Discussion

This section discusses the major impacts of the corresponding dimensionless parameters on the thermal profile of a wavy porous fin. The achieved outcomes are presented graphically for the solid wavy fin (SWF) and PWF cases. Graphical outputs were achieved using particular physical parameter ranges, such as $0.2 \leq N_c \leq 0.8$, $1 \leq Nr \leq 4$, $0 \leq N_t \leq 0.3$, $Sh = 0$ (for SWF), and $Sh = 0.2$ (for PWF). The heat transfer rate of the PWF was explored by developing a heat transfer model by implementing an artificial neural network with a differential evolution algorithm.

The considered wavy fin was assumed to dissipate heat from itself to the surrounding environment via surface convection and radiation mechanisms. These heat transmission processes play a key role in the thermal behavior of the fin and are indicated in mathematical forms, which are nondimensional terms. Thus, the impact of dimensionless variables, such as convective–conductive (N_c) and radiative–conductive (Nr) parameters, are envisioned via graphical plots, as shown in Figures 3 and 4.

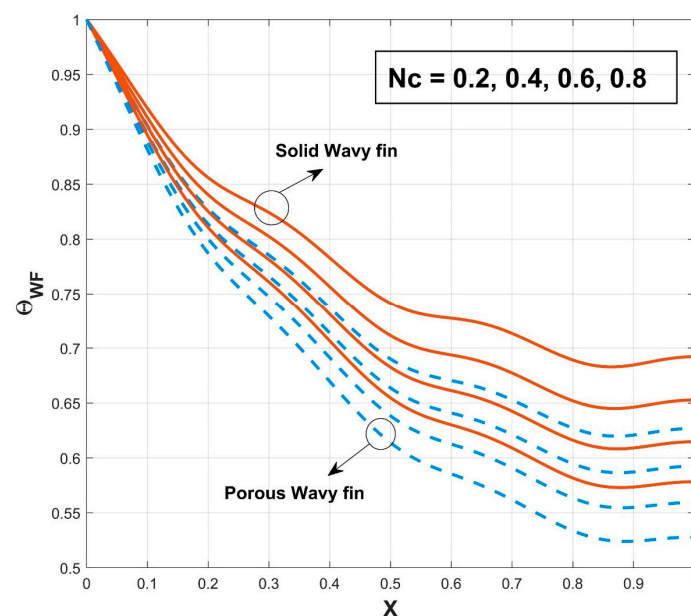


Figure 3. Consequences of N_c on Θ_{WF} of solid and porous wavy fin.

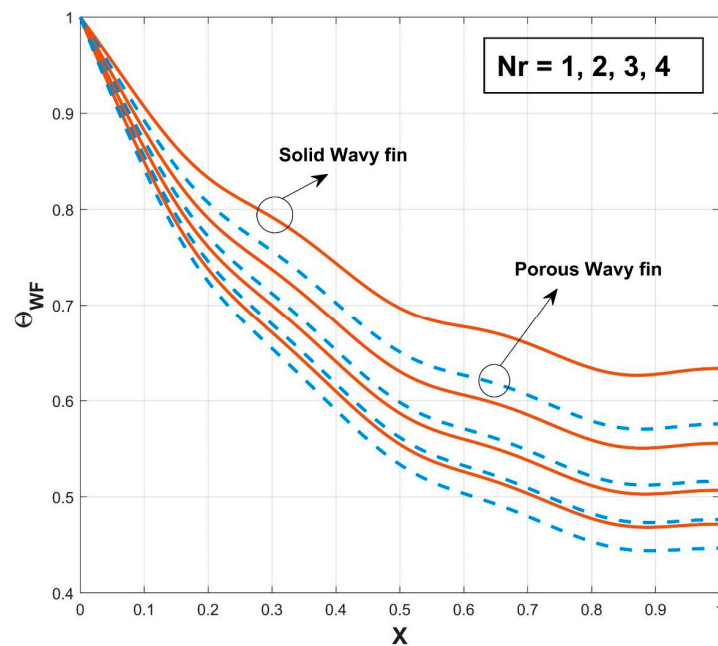


Figure 4. Consequences of N_r on Θ_{WF} of solid and porous wavy fin.

The thermal profile of the wavy extended surface declined with an increasing range of N_c , as revealed in Figure 3. The lessening in the scales of N_r encouraged thermal variation in the fin, as revealed in Figure 4.

The energy loss from the fin, influenced by radiation, was associated with the parameter N_t . Figure 5 explains the variation in the fin's temperature with the influence of N_t for both SWF and PWF cases. The augmented scales of N_t resulted in the thermal distribution decreasing for both circumstances. The variation in the thermal dispersion of the PWF is presented in three-dimensional (3D) graphical form, as shown in Figure 6. The temperature of the fin dispersed from the base to the fin's tip, due to the exclusion of heat caused by the simultaneous mechanisms of radiation and convection.

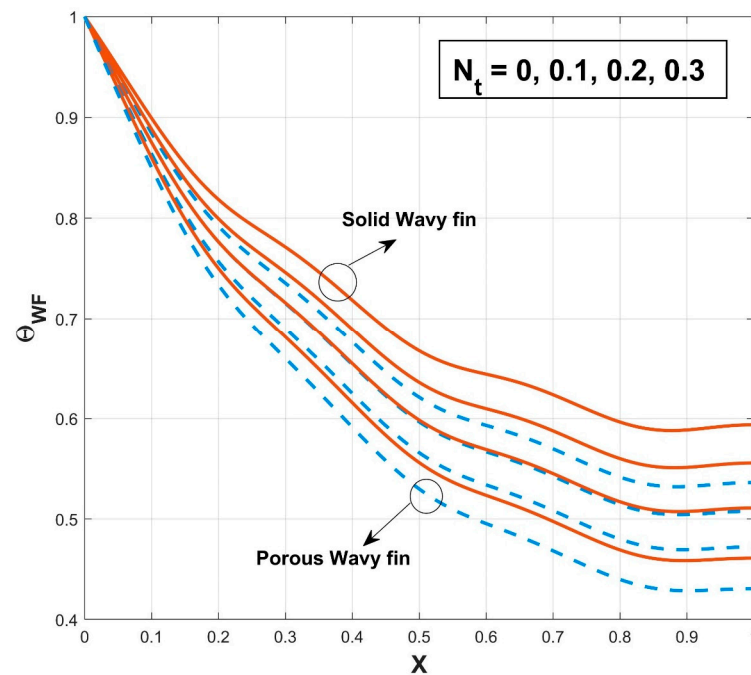


Figure 5. Consequences of N_t on Θ_{WF} of solid and porous wavy fin.

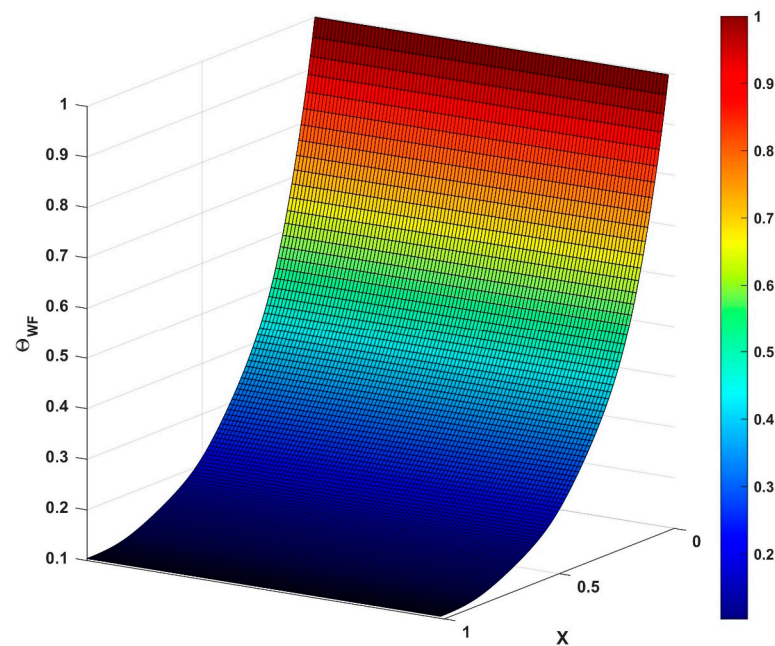


Figure 6. Variation in thermal distribution of the porous wavy fin.

The foremost objective of the investigation was to present the stochastic ANN model for the heat transfer analysis of the PWF by employing the DE-ANN scheme, and the corresponding architecture of the ANN model was represented in terms of thermal parameters, as shown in Figure 7. In this figure, the input layer consists of the data of the thermal parameter, such as (N_c , N_r , Sh , and N_f), whereas the target data includes the heat transfer rate (Q_{WF}) values of the PWF. The ANN adjusts the weights and the number of neurons in the hidden layers, and, here, this was selected by GS and DE algorithms, and both of these were compared. During training, to minimize network loss and learn the complex relationships between the input and output of a given dataset, the training procedure was validated using test data that was not used during training. After training, the network parameters were calculated, allowing the ANN to anticipate unknown inputs and forecast the related output. The parameters selected using DE were a network structure of 24, 17, 8, an adam optimizer with relu activation function, followed by 234 epochs, and a batch size of 33. GS consisted of a network of 10, 10, and 12, to which the optimizer and activation were the same as above, but the epochs were estimated to be 258, with a batch size of 50. Table 1 compares two techniques for parameter estimation in an ANN model. The MSE and Maximum Error (ME) were the performance metrics considered in this table for the training and testing stages. Regarding parameter estimation for the ANN model, the findings clearly show that DE-ANN outperformed GS-ANN. Furthermore, DE-ANN exhibited much lower MSE values for the training and testing phases than GS-ANN. This implies that DE-ANN can accurately estimate the ANN model parameters and deliver more exact predictions. In addition to lowering MSE, DE-ANN performed better in terms of ME. It represented the greatest difference between projected and actual values, and minimizing this error is critical for making accurate forecasts. DE-ANN reduced the maximum error in both the training and testing phases, demonstrating its capacity to grasp complicated patterns and reduce outliers, if present in the data. This was verified by analyzing the following plots and tables.

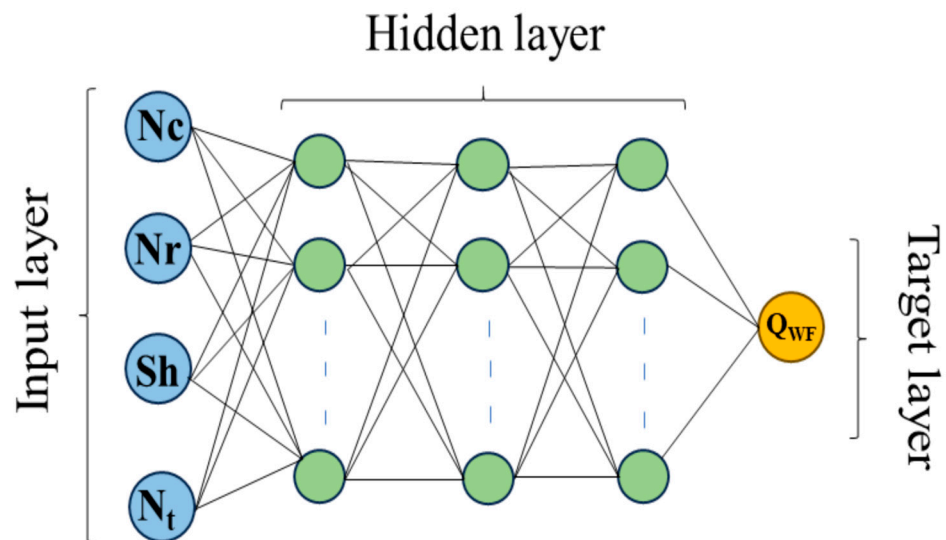


Figure 7. ANN architecture.

Table 1. Performance metrics evaluation.

Model	Training		Testing	
	MSE	ME	MSE	ME
GS-ANN	2.94×10^{-5}	3.82×10^{-2}	2.36×10^{-5}	2.87×10^{-2}
DE-ANN	3.34×10^{-7}	8.43×10^{-5}	2.84×10^{-7}	8.01×10^{-5}

Figure 8 compares the predicted values from the GS-ANN model with the actual values, whereas Figure 9 demonstrates the DE-ANN model's training results. The performance and accuracy of the model's predictions were also evaluated graphically using these plots. These figures show that the applied stochastic DE-based ANN methodology provided more excellent convergent training and testing results than the GS-ANN model. This was authenticated by the values of the training and testing phases. The corresponding R^2 values were closer and equal to one for the DE-ANN model, which confirmed the model's training accuracy. The behavior of the loss function during the training and testing periods is shown in Figure 10. The x-axis indicates training iterations or epochs, and the y-axis represents the loss function value. The training curve displays the evolution of the loss function during the training process, whereas the testing curve depicts its behavior on a separate testing dataset. One of the reasons for the superior performance of DE-ANN lies in its computational efficiency. GS involves an exhaustive search through a predefined grid of parameter combinations, which can be computationally expensive, especially when dealing with a large number of parameters or a wide parameter range. On the other hand, DE operates on population-based optimization, employing a stochastic search strategy to efficiently explore the parameter space, which converges to the optimal solution more quickly. Furthermore, one of the primary benefits of DE over GS for parameter estimation in an ANN model is its resistance to local optima. GS is susceptible to becoming trapped in local optima, which are suboptimal parameter values that keep the algorithm from achieving the global optimum.

This happens because GS endlessly searches through a specified grid of parameter possibilities, restricting its ability to explore the parameter space properly. On the other hand, DE may overcome local optima, due to its population-based strategy and mutation-crossover operations. DE searches a larger parameter space by keeping a population of potential solutions and using stochastic procedures, such as mutation and crossover. This enables it to avoid local optima and search for the global optimum more efficiently. When compared to GS-ANN, the robustness of DE-ANN against local optima improved its

overall performance and estimation accuracy. By avoiding suboptimal solutions, DE-ANN finds more optimal parameter values, resulting in better forecasts and lower errors. This property makes DE-ANN particularly useful when working with complex datasets or high-dimensional parameter spaces. The comparison of performance measures in Table 1 and the evaluation of DE's robustness to local optima demonstrated the effectiveness of DE-ANN in parameter estimation in an ANN model. DE-ANN exhibited greater MSE reduction, maximum error minimization, computational efficiency, and the capacity to avoid becoming caught in local optima. Compared to GS, these benefits establish DE as a more successful technique for predicting optimal parameters in an ANN model.

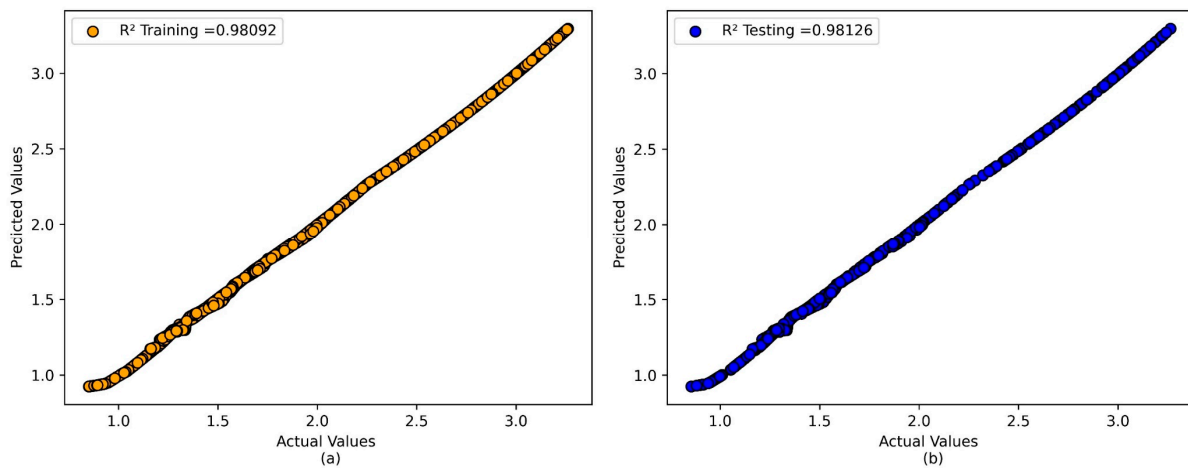


Figure 8. (a) Training prediction plots for GS-ANN (b) Testing prediction plots for GS-ANN.

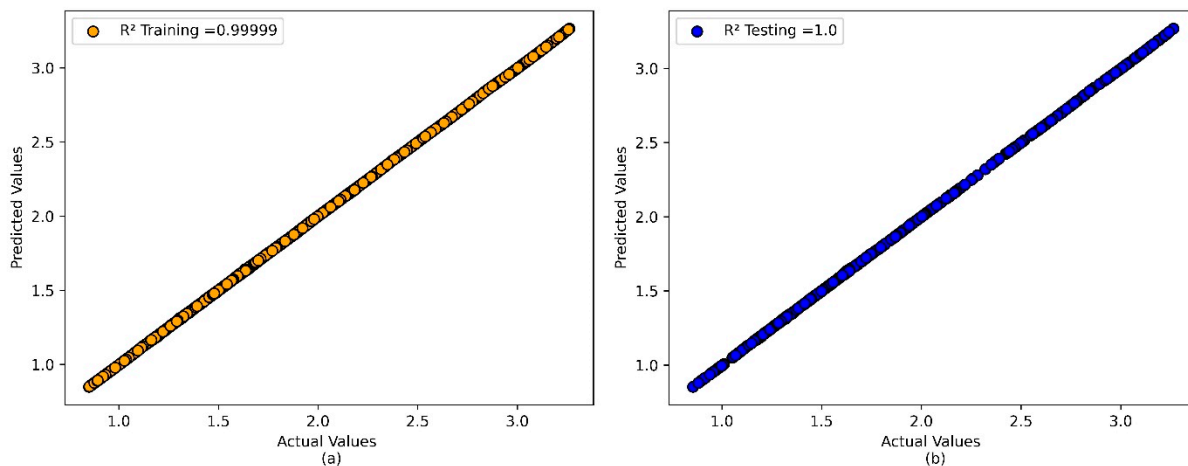


Figure 9. (a) Training prediction plots for DE-ANN (b) Testing prediction plots for DE-ANN.

Figure 11 illustrates the training results of the GS-ANN and DE-ANN target variables plotted against N_c . The ANN models captured the underlying data pattern with surprising efficiency when using DE for the model's hyperparameter estimation. The DE-ANN model precisely matched with the target values, indicating a highly precise fit to the data points. This achievement can be credited to differential evolution's innate capacity to successfully traverse the search space and locate optimal hyperparameters that lead to higher model performance. The GS strategy, on the other hand, had relatively low precision in capturing the intricate correlations between the input and target variables, resulting in a less exact fit to the data.

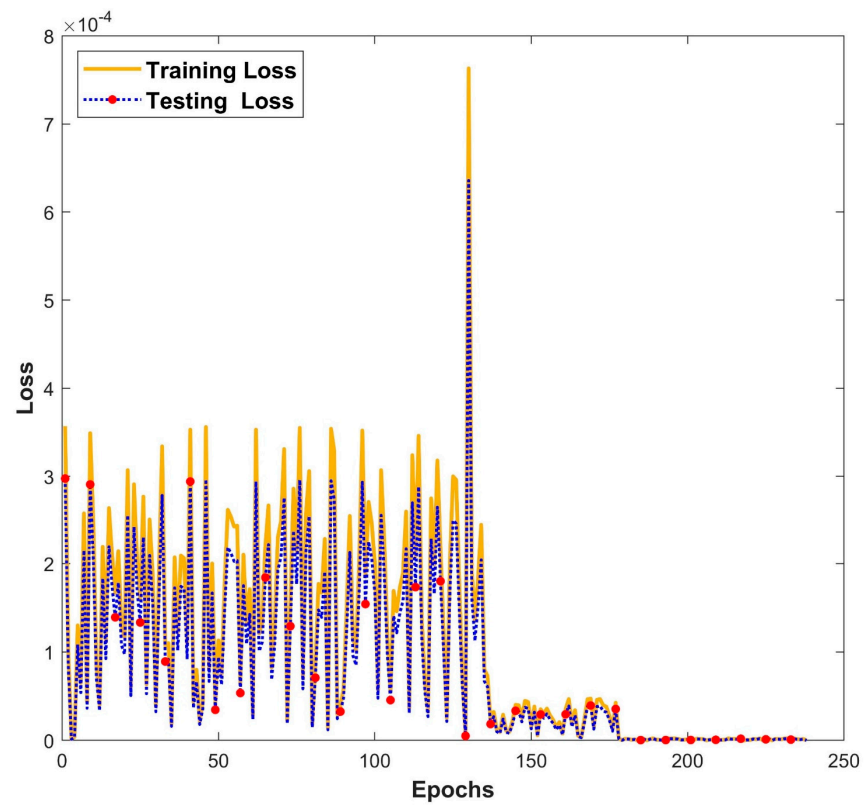


Figure 10. Loss function evaluation plot of DE-ANN.

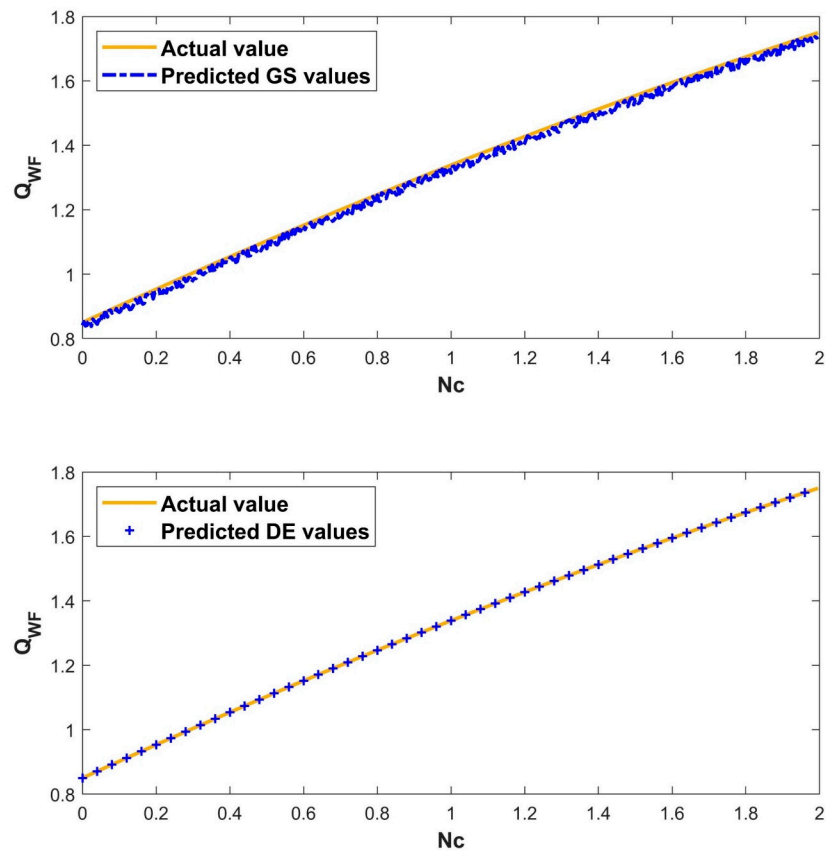


Figure 11. Comparative analysis of GS-ANN and DE-ANN versus N_c values.

The connection between the target variable (Q_{WF}) and Nr is shown in Figure 12. The DE-ANN model yielded an outstanding fit to the target values, mimicking the true data distribution with remarkable fidelity for hyperparameter estimation. Due to its global search capabilities, DE performed better than other methods, since it walks through complicated, high-dimensional spaces and find the best hyperparameters for the ANN model. In contrast, GS found it difficult to fully explore the hyperparameter space, which resulted in a fit that could be better at fully capturing the complex patterns in the data. Figures 13 and 14 present a high correlation between the input variables (Sh and N_t) and the trained result values. As a strong global optimization technique, DE excels at effectively and efficiently exploring the solution space. In both circumstances, it may change its search approach to identify the ideal hyperparameters that accurately capture the data patterns. As a result, the generated curves were very close to the intended values, demonstrating the exceptional fit produced by DE. In contrast, GS can be constrained by its thorough search approach.

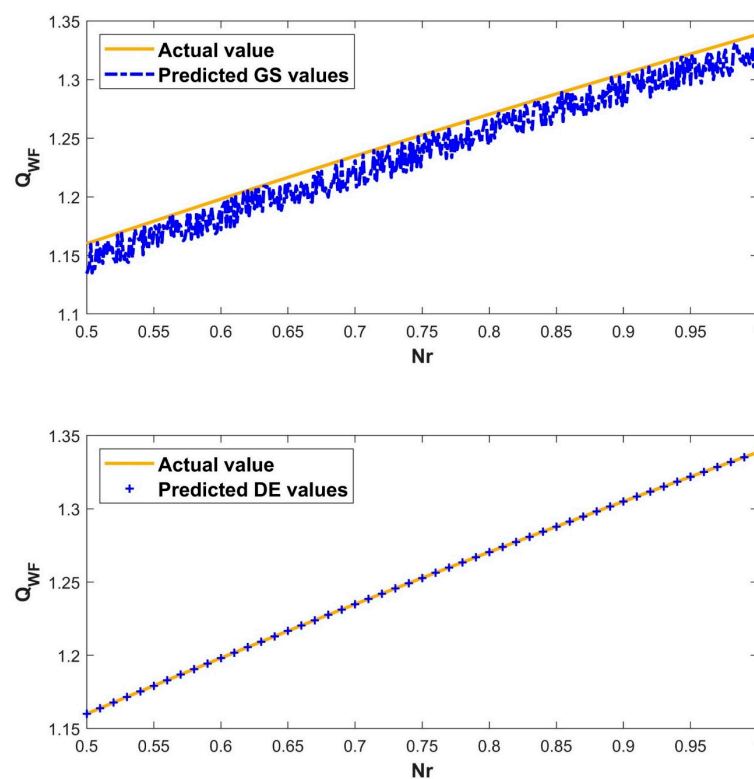


Figure 12. Comparative analysis of GS-ANN and DE-ANN versus Nr values.

The need to quickly navigate the complicated and high-dimensional hyperparameter space resulted in unsatisfactory fits for the above figures. As a result, the GS curves diverged significantly from the intended values, indicating difficulties in capturing the detailed data patterns depicted in the plots. All four figures (Figures 11–14) show that DE consistently outperformed GS in hyperparameter estimation for the ANN model. The capacity of DE to efficiently explore hyperparameter space and adaptively fine-tune model parameters allowed it to obtain highly accurate fits to the target values, accurately capturing the patterns contained in the data. Additionally, GS generated poor results due to its more rigorous and systematic approach, which limited its ability to capture intricate data and, hence, it fell short of precisely fitting the target values.

Tables 2 and 3 highlight the characteristics of the heat transfer rate (Q_{WF}) of the PWF versus varying scales of the thermal parameter of PWF. From these data, it is confirmed that the heat transfer rate of the PWF was augmented with various values of Nc , Nr , N_t ,

and Sh . Moreover, the Q_{WF} values achieved by RKF-45 showed closer convergence with the trained results of Q_{WF} performed by DE-ANN compared to GS-ANN.

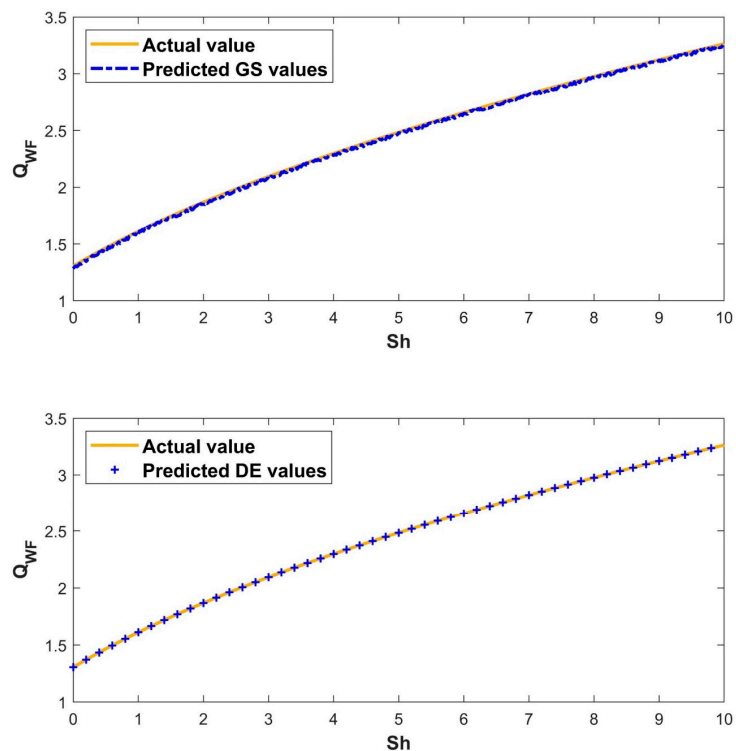


Figure 13. Comparative analysis of GS-ANN and DE-ANN versus Sh values.

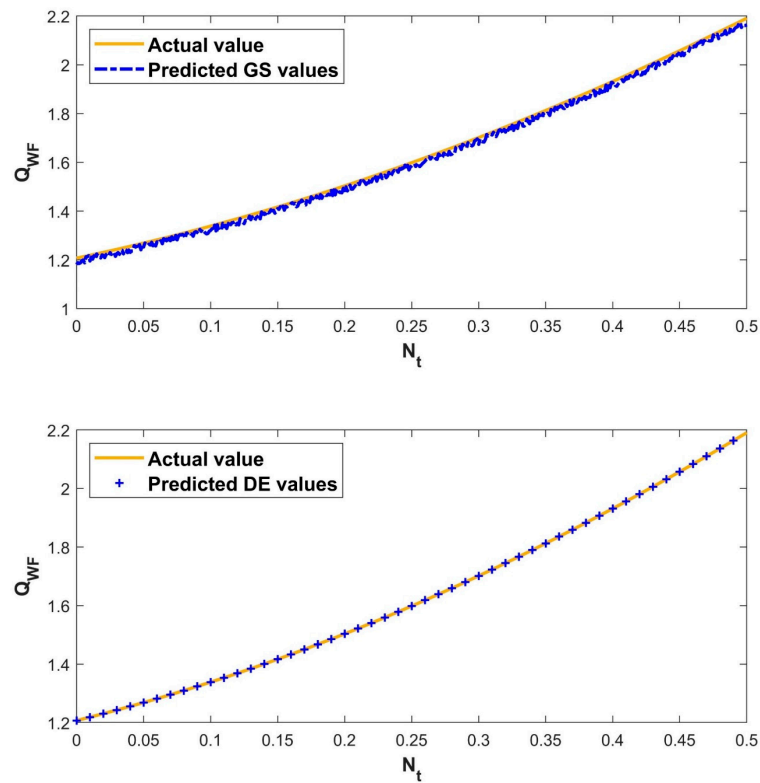


Figure 14. Comparative analysis of GS-ANN and DE-ANN versus N_t values.

Table 2. Evaluation of Q_{WF} (GS-ANN) versus various parameter values.

Nc	Nr	Sh	Nt	Q_{WF} (RKF-45)	Q_{WF} (GS-ANN)	Error
0				0.85011405	0.840990228	0.009123822
0.2				0.95328066	0.94328785	0.00999281
0.4				1.0539614	1.050534536	0.003426864
	0.5			1.1600689	1.134471762	0.025597138
	0.7			1.2348873	1.23078651	0.00410079
	0.9			1.305011	1.295292965	0.009718035
		0		1.3049402	1.28276164	0.02217856
		2		1.8682498	1.850384554	0.017865246
		4		2.2973224	2.280442338	0.016880062
			0	1.2073227	1.180933459	0.026389241
			0.3	1.7016177	1.673833355	0.027784345
			0.5	2.1908957	2.163965102	0.026930598

Table 3. Evaluation of Q_{WF} (DE-ANN) versus various parameter values.

Nc	Nr	Sh	Nt	Q_{WF} (RKF-45)	Q_{WF} (DE-ANN)	Error
0.1				0.90198715	0.90195635	0.0000308156
0.5				1.1032758	1.1032435	0.0000323278
1.0				1.3385787	1.338533	0.000045695
1.5				1.5542698	1.5542114	0.0000583956
2.0				1.7511475	1.7510726	0.0000748647
	0.60			1.1981278	1.19811899	0.00000880819
	0.65			1.2166612	1.2166363	0.0000248735
	0.70			1.2348873	1.2348065	0.0000808085
	0.75			1.2528216	1.2527606	0.0000610428
	0.80			1.2704784	1.270429	0.0000494225
		1		1.6111099	1.6110987	0.0000111584
		3		2.0938689	2.093848	0.0000208749
		5		2.4841792	2.484161	0.0000181909
		7		2.8213522	2.8213307	0.0000214986
		9		3.1230257	3.1229542	0.0000714896
			0.1	1.3385787	1.33856911	0.00000958838
			0.2	1.5034813	1.5034201	0.0000611585
			0.3	1.7016177	1.70161562	0.0000020828
			0.4	1.9314589	1.9314027	0.0000562394
			0.5	2.1908957	2.1908335	0.0000622346

5. Conclusions

This research explores the variation in thermal dispersion in a wavy porous fin under the impacts of convection and radiation. A hybrid forecasting model to estimate the heat transfer rate of the PWF is suggested, which uses the DE technique to determine the parameters in the ANN model. The key results of the present study demonstrate the following:

1. The effect of convective heat exchange is prominent in the distribution of temperature through the fin inducing the decremental change of temperature dispersion in the PWF with variation of the convective–radiative parameter.
2. Radiation heat transmission impacts the fin’s overall heat transfer rate, leading to a reduction in the thermal distribution through PWF.
3. The wavy structured porous fin provides more heat transfer than the solid wavy fin.
4. The heat transfer rate estimated by the intelligent DE-ANN model outperforms the GS-ANN model, due to its high non-linear fitting ability.
5. The DE-ANN forecasting model has consistent performance, whereas conventional ANN models (such as GS-ANN), that are not thoroughly designed, can easily overfit.
6. The DE technique can select the appropriate ANN model parameters, potentially improving prediction accuracy, and capturing growing curve patterns more easily.

DE outperforms GS for ANN model parameter estimation because of its population-based methodology, mutation-crossover procedures, computing efficiency, and robustness to local optima. DE effectively searches the parameter space, responds to data patterns adaptively, converges faster, and makes more accurate predictions. Thus, DE can be employed as a powerful and efficient technique to optimize the parameters of ANN models, which can be beneficial in solving engineering problems.

Author Contributions: Conceptualization, R.S.V.K. and N.A.S.; methodology, C.K.; software, R.S.V.K.; validation, K.V.N., P.N. and S.A.; formal analysis, A.V.; investigation, R.S.V.K.; resources, S.A.; data curation, C.K.; writing—original draft preparation, R.S.V.K.; writing—review and editing, S.A.; visualization, A.V.; supervision, N.A.S.; project administration, K.V.N.; funding acquisition, N.A.S. All authors have read and agreed to the published version of the manuscript.

Funding: This project was supported by Researchers Supporting Project number (RSPD2023R909), King Saud University, Riyadh, Saudi Arabia.

Data Availability Statement: Not applicable.

Acknowledgments: We appreciate Researchers Supporting Project number (RSPD2023R909), King Saud University, Riyadh, Saudi Arabia.

Conflicts of Interest: The authors declare no conflict of interest.

Nomenclature

A	fin’s area
a_{RL}	fin profile aspect ratio
c_p	specific heat
g	acceleration due to gravity
g_c	generation count
H	fin half height
H_0	fin base half height
h^*	convective heat transfer coefficient
K	permeability
k	thermal conductivity
L	fin’s length
ξ	exponent constant
N_c	convection–conduction parameter
N_r	radiation–conduction parameter
N_t	temperature ratio parameter
n	wave number
Q	heat transfer rate (non-dimensional)
q	heat transfer rate
T	temperature

X	fin's length (dimensionless)
x	fin axial distance
<i>Greek symbols</i>	
β	volumetric expansion index
δ	surface wave dimensionless amplitude
ϵ^*	emissivity
Θ	non-dimensional temperature
ν	kinematic viscosity
ρ	density
σ	Stefan–Boltzmann constant
φ	surface wave phase shift
ϕ	porosity
<i>Subscript</i>	
AMB	ambient
B	base
CS	cross-sectional
eff	effective
f	fluid
PWF	porous wavy fin
r	relative quantity
Sd	solid
SF	surface area
WF	wavy fin

References

- Jo, J.; Kim, J.; Kim, S.J. Experimental Investigations of Heat Transfer Mechanisms of a Pulsating Heat Pipe. *Energy Convers. Manag.* **2019**, *181*, 331–341. [[CrossRef](#)]
- Hu, C.; Sun, M.; Xie, Z.; Yang, L.; Song, Y.; Tang, D.; Zhao, J. Numerical Simulation on the Forced Convection Heat Transfer of Porous Medium for Turbine Engine Heat Exchanger Applications. *Appl. Therm. Eng.* **2020**, *180*, 115845. [[CrossRef](#)]
- Hassan, H.; Shafey, N.Y.A. 3D Study of Convection-Radiation Heat Transfer of Electronic Chip inside Enclosure Cooled by Heat Sink. *Int. J. Therm. Sci.* **2021**, *159*, 106585. [[CrossRef](#)]
- Prakash, O.; Singh, S.N. Experimental and Numerical Study of Mixed Convection with Surface Radiation Heat Transfer in an Air-Filled Ventilated Cavity. *Int. J. Therm. Sci.* **2022**, *171*, 107169. [[CrossRef](#)]
- Zhang, Z.; Lou, C. Thermodynamics Second-Law Analysis in an Unsteady Conduction and Radiation Heat Transfer System with Internal Heat Source. *Int. J. Heat Mass Transf.* **2023**, *203*, 123848. [[CrossRef](#)]
- Ndlovu, P.L. The Significance of Fin Profile and Convective-Radiative Fin Tip on Temperature Distribution in a Longitudinal Fin. *Nano Hybrids Compos.* **2019**, *26*, 93–105. [[CrossRef](#)]
- El Ghandouri, I.; El Maakoul, A.; Saadeddine, S.; Meziane, M. Design and Numerical Investigations of Natural Convection Heat Transfer of a New Rippling Fin Shape. *Appl. Therm. Eng.* **2020**, *178*, 115670. [[CrossRef](#)]
- Li, H.; Hu, C.; He, Y.; Tang, D.; Wang, K.; Huang, W. Effect of Perforated Fins on the Heat-Transfer Performance of Vertical Shell-and-Tube Latent Heat Energy Storage Unit. *J. Energy Storage* **2021**, *39*, 102647. [[CrossRef](#)]
- Luo, L.; Yan, H.; Du, W.; Su, W.; Wang, S.; Huang, D. Numerical Study of a Novel Curved Pin Fin for Heat Transfer Enhancement within Aeroengine Turbine Blade. *Aerosp. Sci. Technol.* **2022**, *123*, 107436. [[CrossRef](#)]
- Dogmaz, M.A.; Safak, I.; Gunes, S.; Reddy, J.N. An Investigation of the Thermal Performance of Functionally Graded Annular Fins on a Horizontal Cylinder Under Natural Convection. *Appl. Therm. Eng.* **2023**.
- Kiwan, S.; Al-Nimr, M.A. Using Porous Fins for Heat Transfer Enhancement. *J. Heat Transf.* **2001**, *123*, 790–795. [[CrossRef](#)]
- Ndlovu, P.L.; Moitsheki, R.J. Steady State Heat Transfer Analysis in a Rectangular Moving Porous Fin. *Propuls. Power Res.* **2020**, *9*, 188–196. [[CrossRef](#)]
- Emamifar, A.; Moghadasi, H.; Noroozi, M.J.; Saffari, H. Transient Analysis of Convective-Radiative Heat Transfer through Porous Fins with Temperature-Dependent Thermal Conductivity and Internal Heat Generation. *J. Therm. Eng.* **2022**, *8*, 656–666. [[CrossRef](#)]
- Das, R.; Kundu, B. Simultaneous Estimation of Heat Generation and Magnetic Field in a Radial Porous Fin from Surface Temperature Information. *Int. Commun. Heat Mass Transf.* **2021**, *127*, 105497. [[CrossRef](#)]
- Xuan Hoang Khoa, L.; Pop, I.; Sheremet, M.A. Numerical Simulation of Solid and Porous Fins' Impact on Heat Transfer Performance in a Differentially Heated Chamber. *Mathematics* **2022**, *10*, 263. [[CrossRef](#)]
- Abbas, M.M.; Torabi, M.; Jain, A. Transient Thermal Management Characteristics of a Porous Fin with Radially Outwards Fluid Flow. *Int. J. Heat Mass Transf.* **2023**, *214*, 124435. [[CrossRef](#)]
- Altun, A.H.; Ziylan, O. Experimental Investigation of the Effects of Horizontally Oriented Vertical Sinusoidal Wavy Fins on Heat Transfer Performance in Case of Natural Convection. *Int. J. Heat Mass Transf.* **2019**, *139*, 425–431. [[CrossRef](#)]

18. Luo, C.; Wu, S.; Song, K.; Hua, L.; Wang, L. Thermo-Hydraulic Performance Optimization of Wavy Fin Heat Exchanger by Combining Delta Winglet Vortex Generators. *Appl. Therm. Eng.* **2019**, *163*, 114343. [[CrossRef](#)]
19. Chimres, N.; Chittiphalsri, T.; Asirvatham, L.G.; Dalkılıç, A.S.; Mahian, O.; Wongwises, S. Experimental and Numerical Studies on Heat Transfer Enhancement for Air Conditioner Condensers Using a Wavy Fin with a Rectangular Winglet. *J. Mech. Sci. Technol.* **2020**, *34*, 4307–4322. [[CrossRef](#)]
20. Boland, S.; Majidi, S. Thermal Improvement in Double-Layered Microchannel Heat Sink with Incorporating Wavy Porous Fins. *Heat Transf. Eng.* **2022**, *43*, 485–502. [[CrossRef](#)]
21. Okon, J.O.; Effiom, S.O. Numerical Simulation of the Thermal Performance of a Wavy Fin Configuration for a Straight Fin Array. *Sci. Afr.* **2022**, *16*, e01265. [[CrossRef](#)]
22. Alizadeh, R.; Mohebbi Najm Abad, J.; Fattahi, A.; Alhajri, E.; Karimi, N. Application of Machine Learning to Investigation of Heat and Mass Transfer Over a Cylinder Surrounded by Porous Media—The Radial Basic Function Network. *J. Energy Resour. Technol.* **2020**, *142*, 112109. [[CrossRef](#)]
23. Krishnayatra, G.; Tokas, S.; Kumar, R. Numerical Heat Transfer Analysis & Predicting Thermal Performance of Fins for a Novel Heat Exchanger Using Machine Learning. *Case Stud. Therm. Eng.* **2020**, *21*, 100706. [[CrossRef](#)]
24. Yang, L.; Wang, Q.; Rao, Y. Searching for Irregular Pin-Fin Shapes for High Temperature Applications Using Deep Learning Methods. *Int. J. Therm. Sci.* **2021**, *161*, 106746. [[CrossRef](#)]
25. Khan, N.A.; Sulaiman, M.; Alshammari, F.S. Heat Transfer Analysis of an Inclined Longitudinal Porous Fin of Trapezoidal, Rectangular and Dovetail Profiles Using Cascade Neural Networks. *Struct Multidisc Optim* **2022**, *65*, 251. [[CrossRef](#)]
26. Nguyen, N.P.; Maghsoudi, E.; Roberts, S.N.; Kwon, B. Shape Optimization of Pin Fin Array in a Cooling Channel Using Genetic Algorithm and Machine Learning. *Int. J. Heat Mass Transf.* **2023**, *202*, 123769. [[CrossRef](#)]
27. Sowmya, G.; Lashin, M.M.A.; Khan, M.I.; Kumar, R.S.V.; Jagadeesha, K.C.; Prasannakumara, B.C.; Guedri, K.; Bafakeeh, O.T.; Mohamed Tag-ElDin, E.S.; Galal, A.M. Significance of Convection and Internal Heat Generation on the Thermal Distribution of a Porous Dovetail Fin with Radiative Heat Transfer by Spectral Collocation Method. *Micromachines* **2022**, *13*, 1336. [[CrossRef](#)]
28. Kumar, R.S.V.; Alsulami, M.D.; Sarris, I.E.; Sowmya, G.; Gamaoun, F. Stochastic Levenberg–Marquardt Neural Network Implementation for Analyzing the Convective Heat Transfer in a Wavy Fin. *Mathematics* **2023**, *11*, 2401. [[CrossRef](#)]
29. Abdulrahman, A.; Gamaoun, F.; Varun Kumar, R.S.; Khan, U.; Singh Gill, H.; Nagaraja, K.V.; Eldin, S.M.; Galal, A.M. Study of Thermal Variation in a Longitudinal Exponential Porous Fin Wetted with TiO₂–SiO₂/ Hexanol Hybrid Nanofluid Using Hybrid Residual Power Series Method. *Case Stud. Therm. Eng.* **2023**, *43*, 102777. [[CrossRef](#)]
30. Cui, W.; Si, T.; Li, X.; Li, X.; Lu, L.; Ma, T.; Wang, Q. Heat Transfer Analysis of Phase Change Material Compositated with Metal Foam-Fin Hybrid Structure in Inclination Container by Numerical Simulation and Artificial Neural Network. *Energy Rep.* **2022**, *8*, 10203–10218. [[CrossRef](#)]
31. Suresh Goud, J.; Srilatha, P.; Varun Kumar, R.S.; Sowmya, G.; Gamaoun, F.; Nagaraja, K.V.; Singh Chohan, J.; Khan, U.; Eldin, S.M. Heat Transfer Analysis in a Longitudinal Porous Trapezoidal Fin by Non-Fourier Heat Conduction Model: An Application of Artificial Neural Network with Levenberg–Marquardt Approach. *Case Stud. Therm. Eng.* **2023**, *49*, 103265. [[CrossRef](#)]
32. Motahar, S. Experimental Study and ANN-Based Prediction of Melting Heat Transfer in a Uniform Heat Flux PCM Enclosure. *J. Energy Storage* **2020**, *30*, 101535. [[CrossRef](#)]
33. Varun Kumar, R.S.; Alsulami, M.D.; Sarris, I.E.; Prasannakumara, B.C.; Rana, S. Backpropagated Neural Network Modeling for the Non-Fourier Thermal Analysis of a Moving Plate. *Mathematics* **2023**, *11*, 438. [[CrossRef](#)]
34. Tikadar, A.; Kumar, S. Investigation of Thermal-Hydraulic Performance of Metal-Foam Heat Sink Using Machine Learning Approach. *Int. J. Heat Mass Transf.* **2022**, *199*, 123438. [[CrossRef](#)]
35. Storn, R. Differential Evolution—a Simple and Efficient Adaptive Scheme for Global Optimization over Continuous Spaces. *Tech. Rep. Int. Comput. Sci. Inst.* **1995**, *11*, 20000924911.
36. Centeno-Telleria, M.; Zulueta, E.; Fernandez-Gamiz, U.; Teso-Fz-Betoño, D.; Teso-Fz-Betoño, A. Differential Evolution Optimal Parameters Tuning with Artificial Neural Network. *Mathematics* **2021**, *9*, 427. [[CrossRef](#)]
37. Atangana Njock, P.G.; Shen, S.-L.; Zhou, A.; Modoni, G. Artificial Neural Network Optimized by Differential Evolution for Predicting Diameters of Jet Grouted Columns. *J. Rock Mech. Geotech. Eng.* **2021**, *13*, 1500–1512. [[CrossRef](#)]

Disclaimer/Publisher’s Note: The statements, opinions and data contained in all publications are solely those of the individual author(s) and contributor(s) and not of MDPI and/or the editor(s). MDPI and/or the editor(s) disclaim responsibility for any injury to people or property resulting from any ideas, methods, instructions or products referred to in the content.